International Journal of Minerals, Metallurgy and Materials
Volume 20, Number 10, October 2013, Page 931
DOI: 10.1007/s12613-013-0817-1

Carbothermal reduction process of the Fe-Cr-O system

Yan-ling Zhang, Yang Liu, and Wen-jie Wei

State Key Laboratory of Advanced Metallurgy, University of Science and Technology Beijing, Beijing 100083, China
(Received: 4 December 2012; revised: 17 February 2013; accepted: 22 February 2013)

Abstract: Understanding the reduction behaviors and characteristics of the end products of Fe-Cr-O systems is very important not only for maximizing the recovery of metals from stainless steel dust but also for the subsequent reuse in metallurgical process. The present work first predicted the possible products thermodynamically when $FeCr_2O_4$ was reduced by C. The reduction behaviors by graphite of three kinds of Fe-Cr-O systems, i.e., $FeCr_2O_4$, Fe_2O_3+Cr_2O_3, and Fe+Cr_2O_3, were then investigated in 1350-1550°C. Further, the microstructures of final products and element distribution conditions were examined. The results suggest that, thermodynamically, the mass of products for the carbothermal reduction of $FeCr_2O_4$ is a strong function of temperature, and the initial carbon content is used. More Fe-Cr-C solution and less residual carbon content are obtained at higher temperatures and lower n_C:n_O ratios (the initial molar ratio of C to O in the sample). Experimental data show that the sample amount tends to affect the reduction rate, and the residual carbon content strongly depends on n_C:n_O. With regard to the phases present in products during the reaction process, metal carbides tend to form in the initial stage, whereas Fe-Cr-C solution forms when the degree of reduction is sufficiently high.

Keywords: stainless steel; dust; ternary systems; carbothermal reduction; reaction kinetics

1. Introduction

The Fe-Cr-O system is widespread in the byproducts of stainless steel-making process, such as steel dust, slag, and pickling sludge. With the rapid development of the stainless steel industry in China, a large amount of such byproducts is being generated. Studies have shown that 18-33 $kg{\cdot}t^{-1}$ steel dust is generally produced during the stainless steel-making process [1-3], in which Fe, Cr, and Ni contents are 40wt%-60wt%, 8wt%-15wt%, and 3wt%-9wt%, respectively. To effectively control the recovery of these metals, it is essential to understand the reduction behaviors of such multimetals, coexisting in a single system, and the mechanism of interaction with each other.

Many previous studies on the reduction of Cr_2O_3 by C [4-5], other metals (like Al [6]), or iron-carbon melt [7-8], have reported the effects of some influence factors, such as temperature, sample amount, and the initial carbon content, on the reduction degree and reaction rate together with the possible mechanism and rate-controlling step. In addition, some papers have reported the effects of additives, such as CaF_2, lime, and silicon, on the reduction of Cr_2O_3 in a slag system [8-10]. However, available data are limited on the reduction of mixtures of Fe and Cr oxides, coexisting in a single system, especially for data on the mechanisms of interactions between oxides and the characteristics of possible end products, including the phase compositions, morphologies, element distributions, and residual contents of impurities. These are important basic knowledge not only for maximizing the recovery of metals from stainless steel dust but also for its subsequent reuse within the metallurgical industry. Especially, the residual content of impurities, such as carbon, is a key factor and highly correlated with the application of this recovered materials (reduction products), the lower residual contents of impurities, the higher possibilities of being used as raw materials for alloying, and the less negative impact on the reduction process as raw materials.

Khedr [11] studied the isothermal reduction of fired 0-10wt% Cr_2O_3-doped Fe_2O_3 pellets by H_2 at 900-1200°C. The data suggested that Cr_2O_3 significantly affected the reduction rate of Fe_2O_3. In the initial stage, the rate-controlling step tended to be the interfacial chemical reac-

Corresponding author: Yan-ling Zhang E-mail: zhangyanling@metall.ustb.edu.cn

tion; while in the final stages, the mixed control by solid-state diffusion and interfacial chemical reaction became the rate-controlling step. Takano *et al.* [12] studied the carbothermal reduction of chromites in self-reducing agglomerates and suggested that, in the initial stage, the reaction rate before slag formation was higher due to the gas/solid indirect reaction, but in the later stage, the reduction rate became lower, possibly due to the slower slag/metal direct reaction. Sui *et al.* [13] investigated the selective extraction of Cr, Ni, and Zn from the stainless steel dust, the results revealed that the optimum extraction temperature of Fe-Cr alloys was 1550°C and the separation of slag and metal was good. Sundar Murti and Seshadari [14] studied the reduction of synthetic chromite (~75wt% Cr_2O_3-Fe_2O_3) with carbon and found that the reduction process was probably controlled by the diffusion of oxygen to the surface in the initial stages of reduction; this led to the metallization of iron in the bulk. The X-ray analysis of partially reduced samples (~25% reduction degree) revealed the presence of $FeCrO_3$, Cr_2O_3, Fe, and excess graphite, whereas no carbide formation was detected. Chakraborty *et al.* [15] investigated the carbothermal reduction of chromite ores and found that iron was almost completely reduced before the reduction of chromium in the ore commenced.

The present work first predicted the possible products for the carbothermal reduction of $FeCr_2O_4$ thermodynamically, which was a typical component of the Fe-Cr-O system. The reduction behaviors of three kinds of Fe-Cr-O systems ($FeCr_2O_4$, Fe_2O_3+Cr_2O_3, and Fe+Cr_2O_3) by graphite were then investigated in 1350-1550°C. The effects of influence factors, such as temperature, sample amount, and the initial carbon content, on the reduction degree and rate were discussed. Finally, possible phases present in the products over time during the reaction process were analyzed, together with the morphologies and element distributions of those phases.

2. Thermodynamics

Thermodynamic calculations were performed on the possible reduction products of $FeCr_2O_4$ by carbon using FactSage. Considering the effects of different influence factors, the calculations were based on the principle of minimizing Gibbs free energy. For the initial compositions in $FeCr_2O_4$-C during this simulation, the content of carbon varied according to the initial molar ratio of C to O (expressed as n_C:n_O in this paper). The thermodynamic database in FactSage was applied, and the possible products were identified (gas phase, liquid phase, pure solid, slag, and spinel) in Ar atmosphere at 900-1600°C under the total pressure of 1.01325×10^5 Pa.

Fig. 1 shows the mass fraction of possible products of $FeCr_2O_4$ reduction by carbon at different temperatures. The mass fraction of reduction products is highly temperature dependent. When the temperature increases, the products appear in the order of $FeCr_2O_4$, Cr_2O_3, metal carbides like Fe_7C_3 and Cr_7C_3, liquid phase termed as Fe-Cr-C solution, and low valence chromium carbide Cr_4C. This reveals that high valence metal carbides, such as Fe_7C_3 and Cr_7C_3, tend to be stable at lower temperatures, while Fe-Cr-C solution is more favored at higher temperatures, together with the transfer from high valence chromium carbides (Cr_7C_3) to the low valence one (Cr_4C). When n_C:n_O is controlled at 0.5, most of the metal carbides decompose, and a large amount of Fe-Cr-C liquid

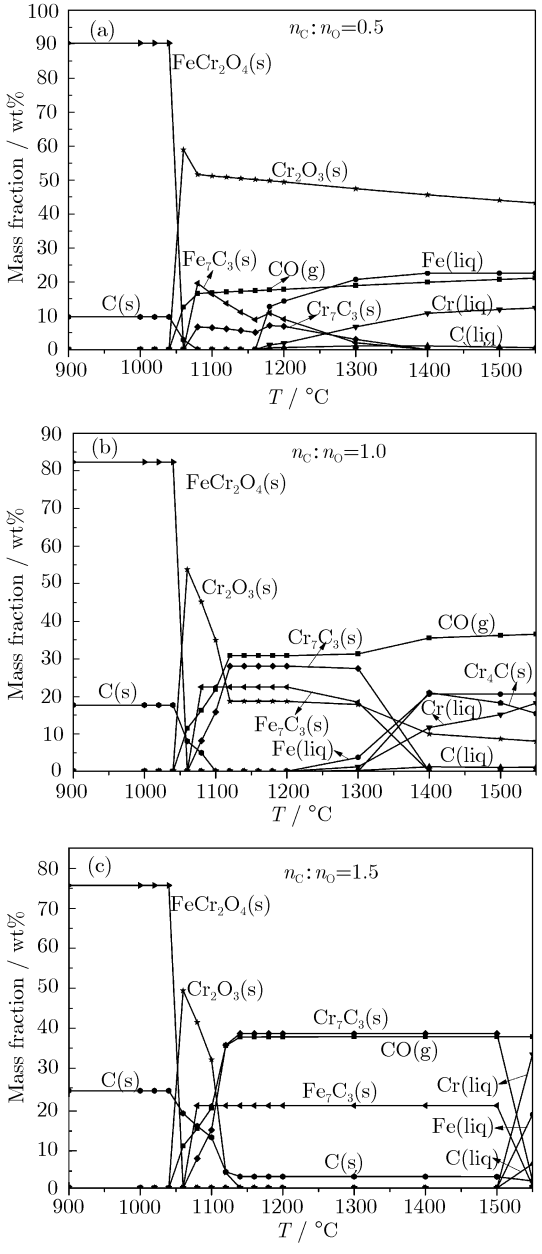

Fig. 1. Mass fraction of possible products for $FeCr_2O_4$ reduction by carbon at different temperatures: (a) n_C:n_O=0.5; (b) n_C:n_O=1.0; (c) n_C:n_O=1.5.

phase is formed at 1200°C (Fig. 1(a)). When n_C:n_O=1.5, the Fe-Cr-C phase does not appear until 1500°C, and the metal carbides are stable in the temperature range as large as 1200-1500°C. Note that when n_C:n_O=1, almost 10% Cr_2O_3 cannot be thermodynamically reduced even at 1550°C (Fig. 1(b)); however, when n_C:n_O=1.5, all of the oxygen can be removed from Cr_2O_3 at 1200°C, as accompanied by the formation of mass chromium carbides (Fig. 1(c)).

Fig. 2 shows the residual carbon content and distribution ratio of metals (Fe and Cr) in the liquid solution and carbides as the functions of temperature (n_C:n_O=1) and n_C:n_O (T=1300°C). The figures suggest that increasing the temperature or decreasing the n_C:n_O mean more Fe-Cr-C solution and fewer metal carbides, while more metal carbides and less Fe-Cr-C solution are obtained at lower temperatures and higher n_C:n_O. Data in Fig. 2 also show that increasing the temperature and decreasing the n_C:n_O tend to decrease the residual carbon content in the system. Correspondingly, the formation of more Fe-Cr solution tends to decrease the residual carbon content, while the formation of metal carbides tends to raise the residual carbon content.

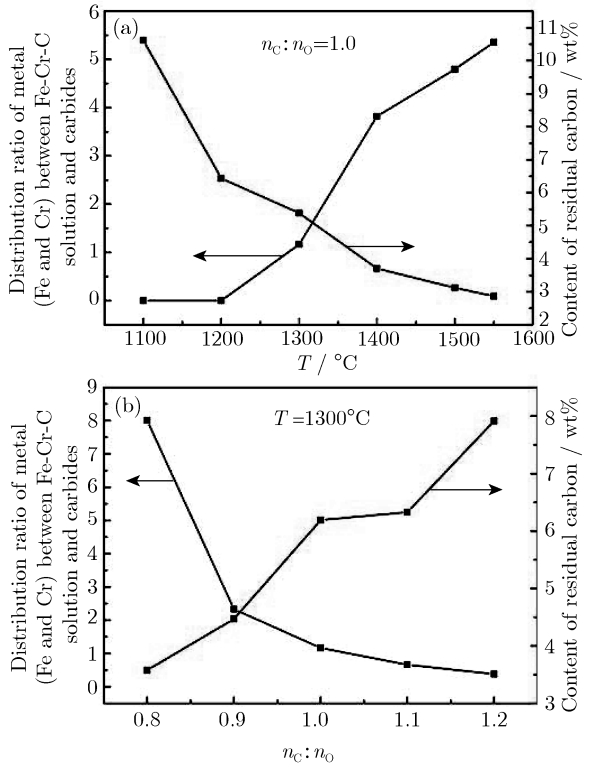

Fig. 2. Residual carbon content and distribution ratio of metals (Fe and Cr) between Fe-Cr-C solution and carbides.

3. Experimental

3.1. Sample

Chemical reagents, such as Cr_2O_3, Fe_2O_3, NiO (purity higher than 99%), metallic Fe powders, and graphite C (purity higher than 99.85%), were employed in the experiments. The mean diameters of these chemical reagents are all less than 74 μm (–200 mesh). $FeCr_2O_4$ was prepared by heating the mixture of Cr_2O_3, Fe_2O_3, and metallic Fe (Cr_2O_3:Fe_2O_3:Fe=3:1:1 by mole) at 1000°C for 5 h under Ar atmosphere in a resistance furnace, which was described in detail in the previous study [16]. For Fe-Cr-O samples, the molar ratio of Fe to Cr was kept at 1:2, and the initial carbon content depended on different experiments. The powders used in the experiments were mixed in a porcelain mortar first, and then, the cylindrical compacts (16 mm in diameter) were formed under a cold isostatic press of 30 MPa for 120 s. The sample weight varied with the cylindrical compact height. The experimental samples and conditions used in this study are shown in Table 1.

3.2. Apparatus

Fig. 3 shows the schematic of experimental apparatus. The main part is a molybdenum-wired resistive furnace equipped with a cracking furnace for NH_3, a temperature-control instrument, a balance with the detection precision of 1 mg, a water-cooling system, and a data-collection system. The temperature in the tube was measured with Pt·30%Rh-Pt·6%Rh thermocouples. The sample pellets were placed in a high-purity aluminum crucible (30 mm in diameter and 30 mm in height), and then hung at the center of the reaction tube by the hook of the precision balance with a molybdenum wire. Before heating, pure Ar (purity higher than 99.999%) gas was injected into the reaction tube from the bottom at a constant flow rate of 1 L/min. After the temperature reached the target value, the crucible containing samples was remained at the upper apart of the reaction tube for about 3 min by hanging at the hook of the balance, and then moved to the center of the reaction tube; this moment was taken as the starting time (0 min). During the holding time, the weight loss of samples was continuously recorded by a data acquisition system; after completing the experiment, the sample was cooled in Ar atmosphere.

3.3. Analysis

The reduction degree of sample (α) was given by

$$\alpha = \Delta W / W_{CO} \tag{1}$$

where ΔW (g) and W_{CO} (g) are the weight loss of the sample and the weight of CO produced after removing all oxygen in the sample, respectively. The residual carbon content (W_C^r) can be obtained through

$$W_C^r = \frac{W_C^0 - 12 \times \dfrac{\Delta W}{28}}{W_S} \times 100\% \tag{2}$$

where W_C^0 (g) and W_S (g) are the initial carbon mass and the sample mass after the experiments, respectively.

Table 1. Experimental samples and conditions

Test No.	Temperature / °C	Sample			
		Compositions	Total weight / g	Molar ratio of Fe to Cr	Molar ratio of C to O	Content of initial carbon / wt%
1	1350	$FeCr_2O_4$ + C	5.43	1:2	1.17	20.00
2	1350	Fe_2O_3 + Cr_2O_3 + C	7.90	1:2	1.07	20.00
3	1350	Fe + Cr_2O_3 + C	9.63	1:2	1.44	20.00
4	1450	$FeCr_2O_4$ + C	5.41	1:2	1.17	20.00
5	1450	Fe_2O_3 + Cr_2O_3 + C	7.61	1:2	1.07	20.00
6	1450	Fe + Cr_2O_3 + C	9.38	1:2	1.44	20.00
7	1550	$FeCr_2O_4$ + C	5.50	1:2	1.17	20.00
8	1550	Fe_2O_3 + Cr_2O_3 + C	7.73	1:2	1.07	20.00
9	1550	Fe + Cr_2O_3 + C	9.92	1:2	1.44	20.00
10	1350	$FeCr_2O_4$ + C	3.01	1:2	1.20	20.50
11	1350	Fe_2O_3 + Cr_2O_3 + C	2.98	1:2	1.20	21.80
12	1350	Fe + Cr_2O_3 + C	3.03	1:2	1.20	17.20
13	1450	$FeCr_2O_4$ + C	3.02	1:2	1.20	20.50
14	1450	Fe_2O_3 + Cr_2O_3 + C	2.91	1:2	1.20	21.80
15	1450	Fe + Cr_2O_3 + C	2.95	1:2	1.20	17.20
16	1550	$FeCr_2O_4$ + C	3.02	1:2	1.20	20.50
17	1550	Fe_2O_3 + Cr_2O_3 + C	3.04	1:2	1.20	21.80
18	1550	Fe + Cr_2O_3 + C	3.06	1:2	1.20	17.20

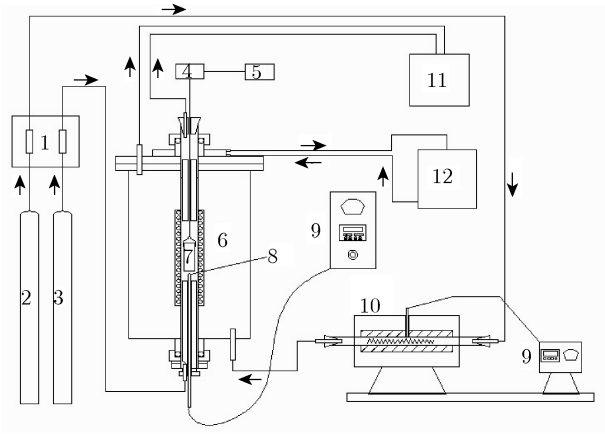

Fig. 3. Schematic of the molybdenum wire furnace: 1—flowmeter; 2—NH_3; 3—Ar; 4—balance; 5—computer for data collection; 6—molybdenum wire furnace; 7—crucible; 8—thermocouple; 9—temperature controller; 10—NH_3-cracking furnace; 11—exhaust; 12—water cooling.

Phases in reduction products were analyzed by X-ray diffraction (XRD, M21X super power X-ray diffraction; Mac Science, Japan). The microscopic morphology and component distribution of products were observed and analyzed by using a scanning electron microscope coupled with an energy dispersive spectrometer (SEM-EDS, JSM-6510/Genesis XM2).

4. Results and discussion

4.1. Influence factors

The reduction degrees of three samples ($FeCr_2O_4$+C, Fe_2O_3+Cr_2O_3+C, and Fe+Cr_2O_3+C) are shown in Fig. 4 as a function of time at different temperatures and initial carbon contents. The hollow-mark represents the data when n_C:n_O is controlled at 1.2, while the solid one shows the data when the initial carbon content is 20wt% and n_C:n_O is different for the different samples. As shown in the figures, the reduction degree of these three samples is highly time and temperature dependent. All of the samples show a similar tendency: the reduction rate linearly increases at the initial stage, then slows down, and levels off. The temperature greatly affects the reduction rate, and the higher the temperature, the shorter the time to reach the maximum reduction degree.

With regard to the effects of other influence factors, Fig. 4(a) shows the reduction degree of $FeCr_2O_4$+C at nearly the same value of n_C:n_O, and the hollow-mark data display a larger reaction rate, especially at a higher temperature. This is probably because that, a smaller sample amount may give a better kinetic condition, such as a smaller diffusion resistance or larger contact area, as shown in Table 1, the weight of the hollow-mark sample was about 3.0 g, while that of the solid-mark sample was about 5.4 g. A much larger sample amount was used for Fe+Cr_2O_3+C when n_C:n_O was controlled to be 1.44 (about 9.4-9.8 g). Hollow-mark data (n_C:n_O=1.2) in Fig. 4(b) show a larger reaction rate, which further validates the tendency observed above: a smaller sample amount means a larger reaction rate. Fig. 4(b) also displays a higher final reduction degree when n_C:n_O=1.44 (solid mark) at the same temperature, which reveals that a larger initial content of carbon tends to raise the final reduction degree of sample. Data in Fig. 4(c) suggest that a larger reaction rate and a higher final reduction degree are simultaneously obtained, as shown in hollow-mark data, where a smaller sample

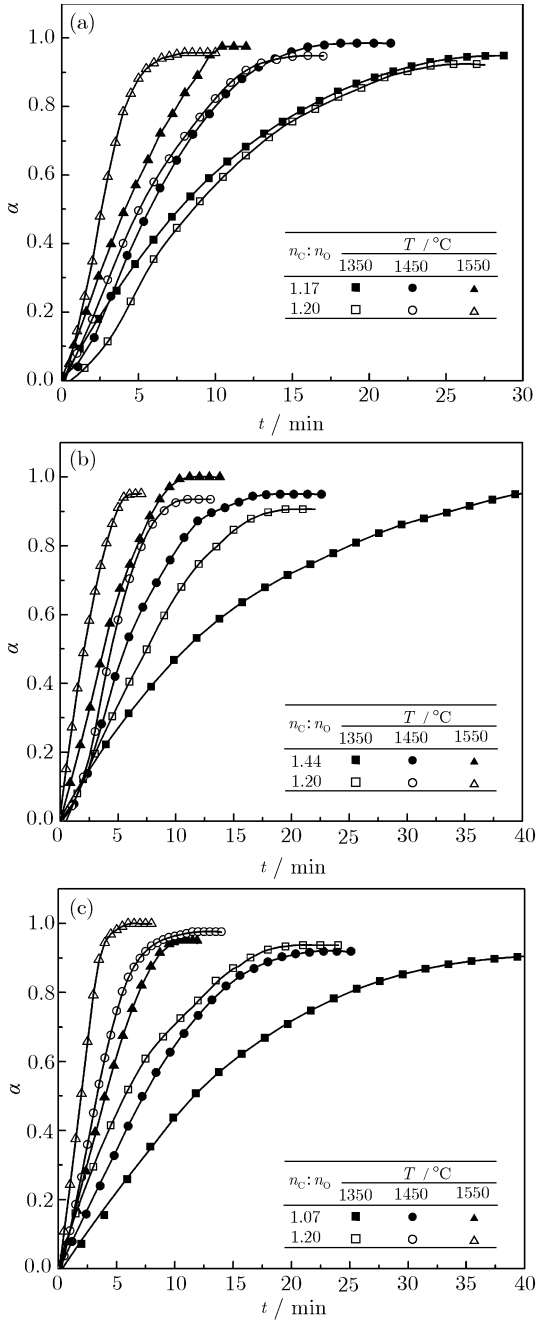

Fig. 4. Reduction curves of the three samples: (a) $FeCr_2O_4$+C; (b) Fe+Cr_2O_3+C; (c) Fe_2O_3+Cr_2O_3+C.

amount (3 g) and more carbon (n_C:n_O=1.2) are used, as shown in Table 1. These results are consistent with data observed in Figs. 4(a) and (b). It can be concluded that the sample amount greatly affects the reaction rate, a larger reaction rate can be obtained for a smaller sample amount; and initial carbon content mainly affects the final reduction degree of sample, which increases with an increase in the content of carbon used.

Fig. 5(a) shows the effects of n_C:n_O on the final reduction degree for all the samples in Table 1. The final reduction degree depends on n_C:n_O and increases with the increase in n_C:n_O. Other factors, such as temperature and sample compositions (or amount), also clearly have some influences since a big fluctuation in the final reduction occurs when n_C:n_O is constant. Fig. 5(b) shows the residual carbon content (W_C^r) in these three samples after reduction as a function of n_C:n_O. The residual carbon content strongly depends on n_C:n_O, and it linearly increases with the increase in n_C:n_O at the same temperature, regardless of the sample amount or the sample type used ($FeCr_2O_4$+C, Fe_2O_3+Cr_2O_3+C, and Fe+Cr_2O_3+C), which means that the effects of other influence factors (such as amount and composition of the sample) on the residual carbon content can be negligible compared with n_C:n_O. Temperature is another important factor that affects the residual carbon content, which tends to decrease with increasing temperature. Hence, the lowest residual carbon content was obtained at the highest temperature and the lowest n_C:n_O, and the largest residual carbon content appeared in the reverse cases. These results agreed well with the thermodynamic predictions, as shown in Figs. 1 and 2.

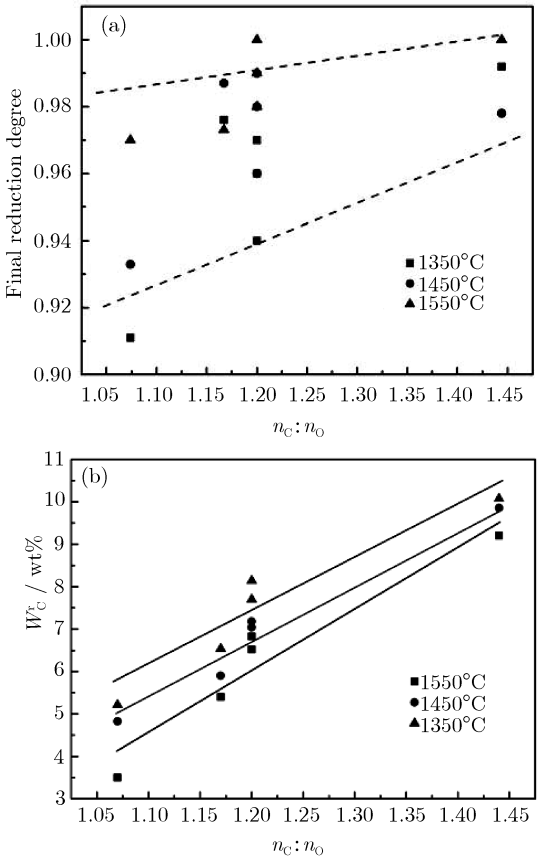

Fig. 5. n_C:n_O dependency of the final reduction degree (a) and residual carbon content (b).

4.2. Kinetic information

As shown in Fig. 4, the reduction degree of each sample linearly increases at the initial stage; this means that the rate constant at this moment is a constant which fits the characteristics of a zero-order reaction. For simplicity, by taking the initial gradient of the reduction degree curve as a rate constant (k, min^{-1}), the Arrhenius plot for sample reduction can be shown in Fig. 6. The apparent activation energies of $FeCr_2O_4$+C, Fe_2O_3+Cr_2O_3+C, and Fe+Cr_2O_3+C samples can then be calculated to be 149.0, 122.4, and 109.9 kJ/mol, respectively. A similar apparent activation energy value (114 kJ/mol) was obtained for the solid-state reduction of chromite pellets with graphite [17].

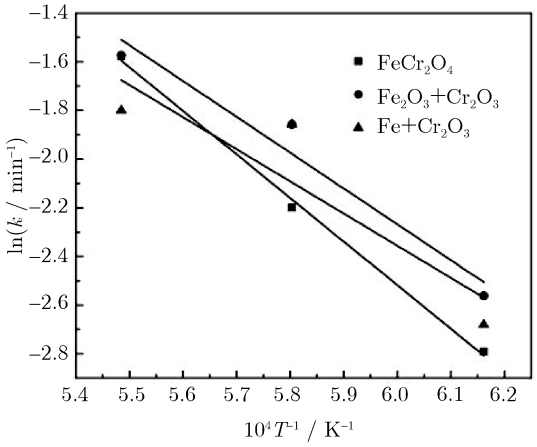

Fig. 6. Arrhenius plot for sample reduction at the initial stage.

4.3. Phase analysis

To examine possible phases in products during the reaction process of Fe-Cr-O systems, experiments with these three samples ($FeCr_2O_4$+20wt%C, Fe_2O_3+Cr_2O_3+20wt%C, and Fe+Cr_2O_3+20wt%C) were carried out. After holding for the target time, the sample was cooled down in Ar atmosphere and analyzed by XRD.

(1) Fe+Cr_2O_3+C sample

Fig. 7 shows the XRD spectra of Fe+Cr_2O_3 sample reduced by carbon over time at 1350°C. It suggests that some chromium carbides are present in the first 5 min (α=38%). Within 20 min, the intensity of carbon greatly decreases, and large amounts of iron and chromium carbides ((Cr, Fe)$_7C_3$) are generated (α=90%) along with the change of high-valence chromium carbide (Cr_3C_2) to the low-valence one (Cr_7C_3). In the first 20 min, the peak of Fe-Cr solid solution does not appear; instead, it is observed at 65 min (α=100%). The final reduction products of Fe+Cr_2O_3 at 1350°C are metal carbides and some amount of Fe-Cr solid solutions.

Based on these results, the main occurrence of the Fe+Cr_2O_3+C system in the initial stage is the formation of metal carbides, as shown in the following equation.

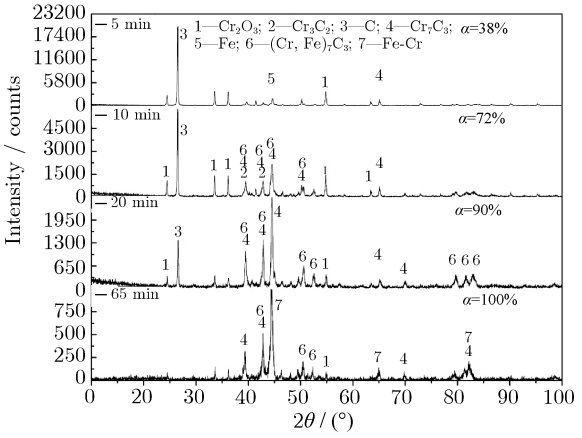

Fig. 7. XRD spectra of Fe+Cr_2O_3 sample reduced by carbon at 1350°C.

$$7Cr_2O_3 + 27C \rightarrow 2Cr_7C_3 + 21CO,\ \Delta G^{\ominus} = -3.636T + 4141.27, \mathrm{kJ \cdot mol^{-1}} \quad (3)$$

The Fe-Cr solution is generated in the later stage through

$$Cr_2O_3 + 3C \rightarrow 2Cr\ (\text{in the form of Fe-Cr solution}) + 3CO,\ \Delta G^{\ominus} = -0.508T + 638.35, \mathrm{kJ \cdot mol^{-1}} \quad (4)$$

or

$$Cr_7C_3 + Cr_2O_3 \rightarrow 9Cr + 3CO,\ \Delta G^{\ominus} = -0.47T + 802.28, \mathrm{kJ \cdot mol^{-1}} \quad (5)$$

The further study reveals that the formation of Fe-Cr solution is mainly through Eq. (5).

In terms of the reduction degree, even when α was as large as 90%, the main reduced products were metal carbides (Cr_7C_3 and (Cr, Fe)$_7C_3$); and the Fe-Cr solution was formed when a much higher reduction degree was obtained.

(2) $FeCr_2O_4$+C sample

Fig. 8 shows the XRD spectra of $FeCr_2O_4$ sample reduced by carbon over time at 1350°C. $FeCr_2O_4$ disappears at 6 min (α=33%) to release a large amount of Cr_2O_3, as shown in the following equation.

$$FeCr_2O_4 + C \rightarrow Fe + Cr_2O_3 + CO,\ \Delta G^{\ominus} = -0.169T + 179.05, \mathrm{kJ \cdot mol^{-1}} \quad (6)$$

At the same time, many metal carbides, such as Cr_7C_3 and (Cr, Fe)$_7C_3$, are formed according to Eq. (3). During the first 10 min (α=70%), the intensity of carbon greatly decreases, while that of Cr_2O_3 and carbides, such as Cr_7C_3 and (Cr, Fe)$_7C_3$, increase. This reveals that the release of Cr_2O_3 from $FeCr_2O_4$ and carburization of Cr/Fe happen almost simultaneously, but the rate of the former is larger than that of the latter. After 10 min, the intensities of Cr_2O_3/carbides (Cr_7C_3 and (Cr, Fe)$_7C_3$) tend to decrease, and a weak peak suggests that a small amount of Fe-Cr solid solution appears at 15 min (α=85%). The final products are Fe-Cr solid solution and metal carbides.

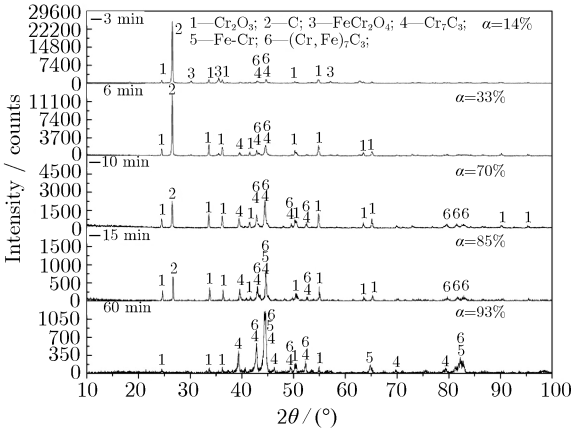

Fig. 8. XRD spectra of $FeCr_2O_4$ sample reduced by carbon over time at 1350°C.

Compared with Fe+Cr_2O_3 sample, the Fe-Cr solution appears earlier with $FeCr_2O_4$.

(3) Fe_2O_3+Cr_2O_3+C sample

Fig. 9 shows the XRD spectra of Fe_2O_3+Cr_2O_3 sample reduced by carbon at 1350°C over time. In the first 6 min (α=52%), the main occurrence is the reduction of Fe_2O_3 to generate Fe_3O_4 and a small amount of metal Fe, as shown in the following equations.

$$3Fe_2O_3 + C \rightarrow 2Fe_3O_4 + CO, \Delta G^{\ominus} = -0.23T + 72.04, \ kJ \cdot mol^{-1} \quad (6)$$

$$Fe_3O_4 + 4C \rightarrow 3Fe + 4CO, \Delta G^{\ominus} = -0.65T + 464.8, \ kJ \cdot mol^{-1} \quad (7)$$

Mass metal carbides like Cr_7C_3 and $(Cr, Fe)_7C_3$ appear after 10 min (α=66%); at 15 min, the peak of carbon almost completely disappears, and the intensity of metal carbides becomes much stronger. Within 15 min (α=88%), Fe-Cr solution is not observed; at 50 min (α=91%), there is clear evidence of the existence of Fe-Cr solution. The final products of Fe_2O_3+Cr_2O_3 are the metal carbides and Fe-Cr solid solution.

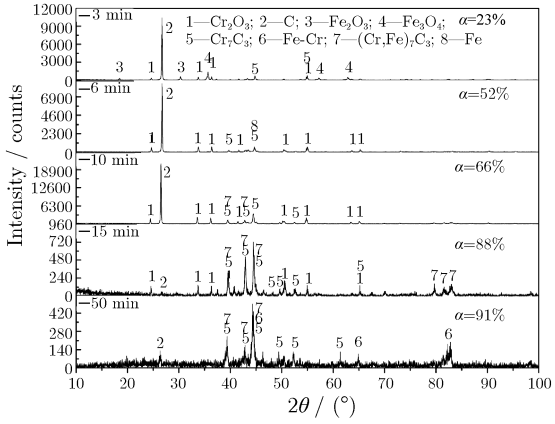

Fig. 9. XRD spectra of Fe_2O_3+Cr_2O_3 sample reduced by carbon over time at 1350°C.

Based on results described above, it can be concluded that the common tendency for reduction of the Fe-Cr-O system was to form metal carbides in the initial stage, and generate the Fe-Cr solution when the reduction degree was sufficiently high. The Fe-Cr solution appeared earliest in $FeCr_2O_4$, and the corresponding reduction degree was 85%; it was not observed when the reduction degrees were 90% and 88% in Fe+Cr_2O_3 and Fe_2O_3+Cr_2O_3 samples, respectively. The generation of Fe-Cr solution seemed to be mainly led by the reaction between metal carbides (iron and chromium carbides) and Cr_2O_3 due to an identical phenomenon, as shown in Figs. 8-10; both of the intensities of Cr_2O_3 and metal carbides (Cr_7C_3 and $(Fe, Cr)_7C_3$) almost simultaneously decreased sharply with the appearance of Fe-Cr solution at the later stage. Mori *et al.* [4] reported a detailed mechanism for the carbothermal reduction of Cr_2O_3, which suggested that, first, several kinds of chromium carbides, such as Cr_3C_2, Cr_7C_3, and $Cr_{23}C_6$, were present, and then, metal Cr was generated from the interaction of chromium carbides and Cr_2O_3. That was consistent with the results of this research.

4.4. Microscopic observation

Scanning electron microscopy coupled with energy dispersive spectrometry (SEM-EDS) was used to further investigate the microscopic morphologies and element distribution among various phases in the final products of carbothermal reduction of the Fe-Cr-O system. The morphologies of the final products of $FeCr_2O_4$+20wt%C sample reduced at 1350°C, Fe_2O_3+Cr_2O_3+20wt%C sample reduced at 1350 °C, $FeCr_2O_4$+20wt%C sample reduced at 1550°C, and Fe_2O_3+Cr_2O_3+20wt%C sample reduced at 1550 °C are shown in Figs. 10(a), (b), (c), and (d), respectively, corresponding to Nos.1, 2, 7, and 8 in Table 1, respectively.

As shown in Fig. 10, the final product of carbothermal reduction of Fe-Cr-O mainly consists of two kinds of phases or materials, a light-colored base matrix and irregularly shaped dark particles. From the perspective of appearance, the former seems to be liquid, and some of the latter (such as particles shown in Figs. 10(a) and (b)) remains solid at the experimental temperatures. On the basis of dendrite structures, other particles in Figs. 10(c) and (d) seem to precipitate from the liquid phase when the sample is cooled. Line analysis and element distribution in Fig. 11 suggest that more Fe and less Cr are distributed in the liquid phase, and the dark particles have higher Cr contents and much lower Fe contents.

Combining these results and XRD analyses shown in Figs. 7-9, it suggests that two kinds of phases are formed during the carbothermal reduction of Fe-Cr-O systems at high temperature, the light-colored Fe-Cr-C liquid base and metal carbides appearing as dark particles, as shown in Fig. 11. More Cr existed as metal carbides and more

Fe is distributed in the Fe-Cr-C solutions together with higher C content in metal carbides during the reduction of Fe-Cr-O systems at high temperature. The primary metal carbides present during reduction tend to remain solid, especially at relatively low reduction temperature, such as 1350°C, because of their high melting point. When the sample is cooled, some of the metal carbides precipitate out of the Fe-Cr-C solution and produce dendrite crystals because the solubility of Cr in solution decreases with decreasing temperature.

Further, as observed in Fig. 10, both $FeCr_2O_4$+C and Fe_2O_3+Cr_2O_3+C systems exhibit similar tendencies, more Fe-Cr-C solution and fewer metal carbide particles are formed with the increase of temperature, which agrees well with thermodynamic predictions in Figs. 1 and 2(a). However, when the two samples are compared, more Fe-Cr-C solution tends to be obtained in Fe_2O_3+Cr_2O_3+20wt%C sample than that in $FeCr_2O_4$+20wt%C sample at each reduction temperature, which may be because of the lower n_C:n_O in the former (i.e., n_C:n_O=1.07 for Fe_2O_3+Cr_2O_3+20wt%C sample and 1.17 for $FeCr_2O_4$+20wt%C sample). This finding is also consistent with thermodynamic predictions in Fig. 2(b), that is, lower n_C:n_O enables the formation of Fe-Cr-C solution. The residual carbon content in Fe_2O_3+Cr_2O_3+20wt%C sample should be correspondingly lower than that in $FeCr_2O_4$+20wt%C sample, since less carbon is distributed throughout the Fe-Cr-C solution than that in metal carbides (as shown in Fig. 11), which is also consistent with experimental results shown in Fig. 5(b).

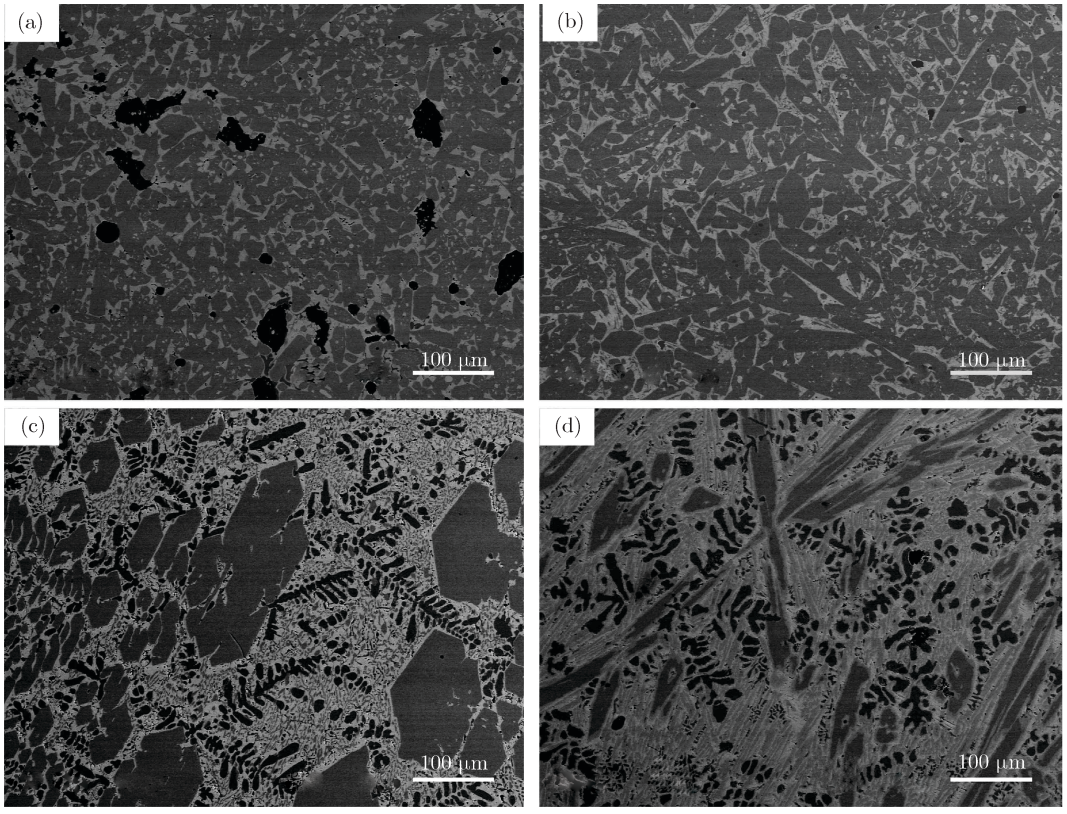

Fig. 10. SEM images of the final products of carbon-reduced Fe-Cr-O systems: (a) $FeCr_2O_4$ reduced at 1350°C; (b) Fe_2O_3+Cr_2O_3 reduced at 1350°C; (c) $FeCr_2O_4$ reduced at 1550°C; (d) Fe_2O_3+Cr_2O_3 reduced at 1550°C.

5. Conclusions

(1) Thermodynamic predictions suggest that the mass fraction of products for the carbothermal reduction of $FeCr_2O_4$ is a strong function of temperature and initial carbon content. More Fe-Cr solution and less residual carbon content can be obtained at higher temperatures and lower n_C:n_O, while more metal carbides and higher residual carbon contents appear in the reverse case.

(2) Experimental data show that sample amount affects the reduction rate of sample, and a larger reaction rate is observed with less sample amount. The n_C:n_O ratio has some influence on the final reduction degree. The residual carbon content strongly depends on n_C:n_O, and it linearly increases with an increase in n_C:n_O at each temperature. The effects of other influence factors on the residual carbon content, such as the amount and composition of the sample, can be ignored compared with that of n_C:n_O.

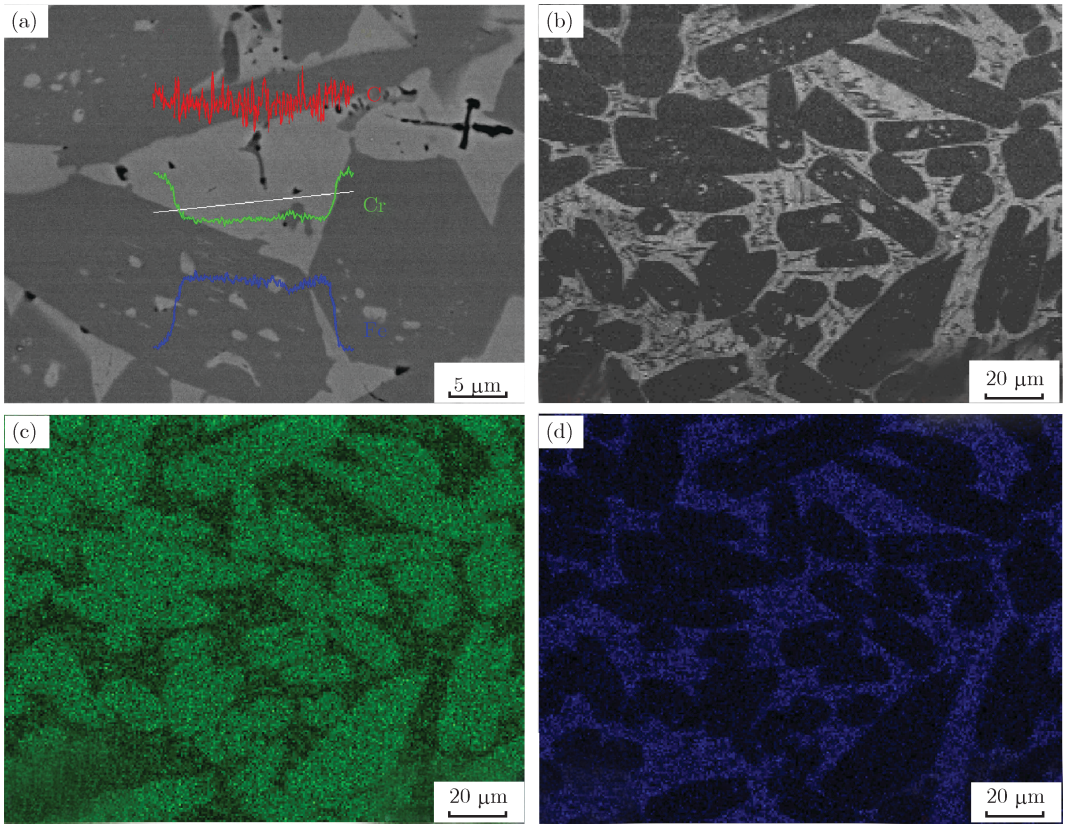

Fig. 11. Line analysis images and element distribution of the final products of Fe_2O_3+Cr_2O_3+C reduced at 1350°C: (a) line analysis image; (b) back scattered electron image; (c) element map of Cr; (d) element map of Fe.

(3) For the reduction of Fe-Cr-O systems, the common tendency is that metal carbides are present at the initial stage, and Fe-Cr solution is generated when the reduction degree is sufficiently high. The generation of Fe-Cr solution is mainly led by the reaction between metal carbides (iron and chromium carbides) and Cr_2O_3.

(4) SEM-EDS observation of microstructure show that the final product of carbothermal reduction of Fe-Cr-O systems mainly consists of two kinds of phases: light-colored Fe-Cr-C solution and metal carbide particles with irregular shape and dark color. More Cr exists in metal carbides, while more Fe is distributed throughout the Fe-Cr-C solution, and the content of C in the former is higher than that in the latter.

Acknowledgments

This work was financially supported by the National Natural Science Foundation of China (No. 51074025) and the Fundamental Research Funds for the Central Universities of China (No. FRF-SD-12-009A).

References

[1] G.J. Ma, W. Fan, Z.H. Xu, Z.L. Xue, W. Wang, and W.H. Su, Distribution behavior of chromium and other elements in the stainless steel plant dust, *Chin. J. Process Eng.*, 10(2010), No. 1, p. 68.

[2] B. Peng and J. Peng, Physical and chemical characteristics of dust from electric arc furnace stainless steelmaking and mechanism of its formation, *J. North China Univ. Technol.*, 15(2003), No. 1, p. 34.

[3] Y.C. Li, X. Yu, Q. Wang, Q.J. Li, and X. Hong, Experimental study on pre-reduction of fine dust from stainless steel making, *Chin. J. Process Eng.*, 10(2010), No. 6, p. 1115.

[4] T. Mori, J. Yang, and M. Kuwabara, Mechanism of carbothermic reduction of chromium oxide, *ISIJ Int.*, 47(2007), No. 10, p. 1387.

[5] B. Peng, H.C. Song, J. Wang, L.Y. Chai, Y.Y. Wang, and X.B. Min, Reduction process of Cr_2O_3/carbon pellets, *J. Cent. South Univ. Sci. Technol.*, 36(2005), No. 4, p. 571.

[6] O. Mitsuyuki Cintho, C. Parra de Lazzari, J.D. Trani Capocchi, Kinetics of the non-isothermal reduction of Cr_2O_3 with aluminium, *ISIJ Int.*, 44(2004), No. 5, p. 781.

[7] R.J. Fruehan, Rate of reduction of Cr_2O_3 by carbon and carbon dissolved in liquid iron alloys, *Metall. Trans. B*, 8(1977), No. 2, p. 429.

[8] T. Nakasuga, H. Sun, K. Nakashima, and K. Mori, Reduction rate of Cr_2O_3 in a solid powder state and in CaO-SiO_2-Al_2O_3-CaF_2 slags by Fe-C-Si melts, *ISIJ Int.*, 41(2001),

No. 9, p. 937.

[9] N. Yoshikawa, K. Mashiko, Y. Sasaki, S. Taniguchi, and H. Todoroki, Microwave carbo-thermal reduction for recycling of Cr from Cr-containing steel making wastes, *ISIJ Int.*, 48(2008), No. 5, p. 690.

[10] Y.L. Ding and N.A. Warner, Catalytic reduction of carbon-chromite composite pellets by lime, *Thermochim. Acta*, 292(1997), No. 1-2, p. 85.

[11] M.H. Khedr, Isothermal reduction kinetics of Fe_2O_3 mixed with 1-10% Cr_2O_3 at 1173-1473 K, *ISIJ Int.*, 40(2000), No. 4, p. 309.

[12] C. Takano, A.P. Zambrano, A.E.A. Nogueira, M.B. Mourao, and Y. Iguchi, Chromites reduction reaction mechanisms in carbon-chromites composite agglomerates at 1773 K, *ISIJ Int.*, 47(2007), No. 11, p. 1585.

[13] Y.F. Sui, G.D. Sun, F. Jin, C.G. Wang, M. Guo, and M. Zhang, Selective extraction of heavy metals Cr, Ni and Zn from stainless steel-making dust, *J. Univ. Sci. Technol. Beijing*, 34(2012), No. 10, p. 1130.

[14] N.S. Sundar Murti and V. Seshadari, Kinetics of reduction of synthetic chromite with carbon, *Trans. Iron Steel Inst. Jpn.*, 22(1982), p. 925.

[15] D. Chakraborty, S. Ranganathan, and S.N. Sinha, Investigations on the carbothermic reduction of chromite ores, *Metall. Mater. Trans. B*, 36(2005), No. 4, p. 437.

[16] W.J. Wei, *Reduction Kinetic of Fe-Ni/Cr-O System* [Dissertation], University of Science and Technology Beijing, Beijing, 2012, p. 57.

[17] Y.L. Ding and N.A. Warner, Kinetics and mechanism of reduction of carbon-chromite composite pellets, *Ironmaking Steelmaking*, 24(1997), No. 3, p. 224.